Theory of strong-field light-induced collisional energy transfer in Eu and Sr

A. Bambini
Istituto di Elettronica Quantistica del Consiglio Nazionale delle Richerche, Via Pianciatichi 56/30 50127 Firenze, Italy

S. Geltman
Joint Institute for Laboratory Astrophysics, University of Colorado, Boulder, Colorado 80309-0440 and National Institute of Standards and Technology, Boulder, Colorado 80309-0440

(Received 31 May 1994)

The theory of light-induced collisional energy transfer (LICET) in the Eu-Sr system is extended to include all the degenerate M states that occur in the separated-atom basis states. Previous treatments were restricted to only the $M = 0$ substates. Numerical solutions are obtained for the resulting nine-state dynamic coupled system to determine transitions probabilities on a given straight-line path. Intense laser fields of linear and circular polarization are treated. It is found that the full M-state treatment results in dependences on the trajectory orientation angles which are much more complex than in the $M = 0$ treatment. The exact and quasisymmetries involving these orientation angles are described in simple group-theoretic terms. The resulting spectral line shapes (LICET transition cross sections as a function of laser detuning) are seen to have structures that are understood in terms of the coupling matrix elements, as well as appreciable Stark shifts. These shifts, which appear to be an essential outcome of the theory, are not yet seen in measurements of the LICET line shape.

PACS number(s): 34.50.Rk

I. INTRODUCTION

Our general understanding of the process of light-induced collisional energy transfer (LICET) has advanced steadily since the process was first proposed by Gudzenko and Yakovlenko [1]. Their two-state atomic representation plus dipole-dipole interaction gave rise to a Lorentzian-like shape for the LICET cross section which varied linearly with the radiation intensity, as a one-photon absorption process should at low intensities. It was then shown by Geltman [2] that at large intensities a saturation of the transition occurred and the peak cross section changed its variation with intensity from $\sim I$ to $\sim I^{1/2}$. A molecular-based treatment by Gallagher and Holstein [3] demonstrated the importance of the van der Waals interaction to the low-intensity line shape, which becomes highly asymmetric. This asymmetry arises from the fact that the initial and final molecular potential curves will allow a region of resonance with the laser photon $\hbar\Omega$ on only one side of the line, called the quasistatic wing, while on the other side (antistatic) the absence of energy conservation results in a very rapid falloff. The quasistatic wing behavior from this picture is $(\Delta\Omega)^{-1/2}$. It was then shown by Bambini and Berman [4] that a two-state basis, even if they are molecular states, is not adequate to describe the far quasistatic wing behavior. They showed that the introduction of a third basis state, which couples collisionally and radiatively with the initial and final states, leads to the quasistatic wing behavior

$$(\Delta\Omega)^{-1/2}(|\Delta_0| + \Delta\Omega)^{-3/2},$$

where Δ_0 is detuning between the intermediate state and the initial or final state. Thus the molecular two-state form is modified for $|\Delta\Omega| \gtrsim |\Delta_0$, and the limiting far wing behavior is $(\Delta\Omega)^{-2}$. A physical interpretation of this effect is that the introduction of the intermediate state, and its adiabatic population during the collision, allows a departure from the two-state quasistatic form. While the above discussion on LICET line shape applies to the case of weak laser fields, or essentially one-photon absorption, a number of studies have looked at the strong-field problem [5,6]. As the field is made more intense, and radiative coupling becomes dominant over collisional coupling, Stark shifts of the line center occur, and the line shape tends to become symmetrical and intensity broadened.

On the experimental side, the first observations of LICET by Harris *et al.* [7] have been followed by extensive weak-field line-shape studies on a number of atomic systems, including Rb-K [8], Na-Ca [9], Li-Sr [10], and Eu-Sr [11]. Those measurements generally confirm the theoretical expectation of asymmetric line shapes and the quasistatic wing transition from $(\Delta\Omega)^{-1/2}$ to $(\Delta\Omega)^{-1/2}$ $(|\Delta_0| + \Delta\Omega)^{-3/2}$ on the far wing. They also confirmed the intensity transition of the peak cross section from I to $I^{1/2}$ behavior. A theoretical expectation [12,13] that was *not* confirmed by the measurements is the Stark shift. A very recent measurement was made by Mazzoni and Fini [14] on the Eu-Sr system in the intensity range $5 \times 10^7 - 3.75 \times 10^9$ W/cm^2. While their results show a trend to decreasing asymmetry as intensity increases, which is consistent with the theory, they do not show the predicted shift in the position of the central peak.

This disagreement between experiment and theory on the question of a shift is at present the major obstacle to a full understanding of the LICET process. As such, it is a leading motivator of the present work. The two previous calculations [12,13] on the Eu-Sr system adopted the simple set of product atomic basis states which included only the $M = 0$ substates. That model was adequate

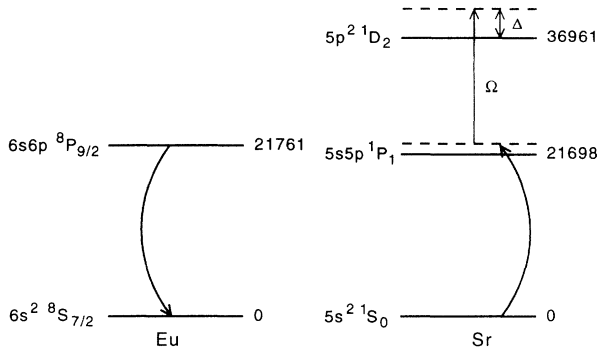

FIG. 1. Simplified atomic energy levels (in cm^{-1}) for the Eu-Sr LICET process. The curved arrows represent the joint collisional transitions.

to explain all the weak-field features of the LICET line shape, and at the same time it predicted a high-field shift of the order of $\sim -0.035\ cm^{-1}/(MW/cm^2)$.

In the present work we retain the same essential set of three basis states:

$$|i\rangle = \mathrm{Sr}(5s^2\ ^1S_0) + \mathrm{Eu}(6s),$$
$$|n\rangle = \mathrm{Sr}(5s5p\ ^1P_1) + \mathrm{Eu}(6s^2\ ^8S_{7/2}),$$
$$|f\rangle = \mathrm{Sr}(5p^2\ ^1D_2) + \mathrm{Eu}(6s^2\ ^8S_{7/2}),$$

but now we include all possible M states. The appropriate energy levels are shown in Fig. 1.

This enlarges our basis set considerably and of course involves much larger amounts of computing time, but we feel that it is necessary to do this as the next step toward the full treatment of the problem.

II. FORMULATION OF THEORY

A. The basis states of the LICET transition

The level structure of europium is complicated by its large spin, $S = 7/2$. This couples to the orbital angular momentum $L = 0$ of two $6s$ electrons to form the ground state, and to the orbital angular momentum $L = 1$ of the $6s6p$ electrons to form a multiplet, with $J = 5/2$, $J = 7/2$, and $J = 9/2$. Initially, we assume that europium is in the $J = 9/2$ excited state.

Since neither the collisional interaction between the two atoms nor the coupling of each atom with the electromagnetic field induces transitions among states with different spin, we can simplify the problem by neglecting the electron spin in the europium atoms, by assuming the two states of europium to be a "$^1S_0$" and a "$^1P_1$" state, respectively. Extensive calculations of LICET transitions involving the whole set of substates in europium have shown that such an approximation does not introduce significant modifications in transition probabilities.

The level structure of strontium is simpler. The two outer electrons of strontium form the ground state ($5s^2\ ^1S_0$), the first excited state ($5s5p\ ^1P_1$), and the double excited state ($5p^2\ ^1D_2$).

We form the set of essential basis states for the LICET transition as the outer product of states of europium and strontium. When magnetic degeneracy is accounted for, the essential states are eleven in all. These states are defined as follows.

The first three states, labeled 1, 2, and 3, are formed by the three magnetic substates of europium "$^1P_1$" and strontium in the $^1S_0$ ground state; states 4, 5, and 6 are formed by europium in the ground state "$^1S_0$" and the three magnetic substates of strontium $^1P_1$. The final five states, 7 through 11, are formed by europium in the ground state and the five magnetic substates of strontium $^1D_2$. The magnetic substates of both europium and strontium are referred to the quantization axis Z which is chosen along the field polarization axis (for linearly polarized field) or along the direction of field propagation (for circularly polarized field).

Denoting by $\mathbf{r}_{a_1}$, $\mathbf{r}_{a_2}$ the coordinates of the two outer electrons in the europium atom and by $\mathbf{r}_{b_1}$, $\mathbf{r}_{b_2}$ the coordinates of the two outer electrons in the strontium atom, we can write the wave vectors of these states as follows:

$$|1,2,3\rangle = \frac{1}{\sqrt{2}}\{u_{6s}(\mathbf{r}_{a_1})u_{6pm}(\mathbf{r}_{a_2}) + u_{6s}(\mathbf{r}_{a_2})u_{6pm}(\mathbf{r}_{a_1})\}\ v_{5s}(\mathbf{r}_{b_1})\ v_{5s}(\mathbf{r}_{b_2}), \tag{1}$$

$$|4,5,6\rangle = u_{6s}(\mathbf{r}_{a_1})\ u_{6s}(\mathbf{r}_{a_2})\ \frac{1}{\sqrt{2}}\ \{v_{5s}(\mathbf{r}_{b_1})v_{5pm}(\mathbf{r}_{b_2}) + v_{5s}(\mathbf{r}_{b_2})v_{5pm}(\mathbf{r}_{b_1})\}, \tag{2}$$

$$|7,8,9,10,11\rangle = u_{6s}(\mathbf{r}_{a_1})\ u_{6s}(\mathbf{r}_{a_2})\ \sum_{m_1 m_2} C(112; m_1 m_2 M)\ v_{5pm_1}(\mathbf{r}_{b_1})\ v_{5pm_2}(\mathbf{r}_{b_2}), \tag{3}$$

where we have indicated by $u(\mathbf{r}_a)$ and $v(\mathbf{r}_b)$ the atomic orbitals of europium and strontium, respectively. In Eq. (3), $C(112; m_1 m_2 M)$ denote the Clebsch-Gordan coefficients of angular momentum coupling.

Within each multiplet, the states are arranged in increasing order of the magnetic quantum number M, so that, for instance, state 1 has $M = -1$, state 2 has $M = 0$, and state 3 has $M = 1$. In the set of final states [Eq. (3)], M ($= m_1 + m_2$) ranges from -2 to $+2$, five states in all. However, as will be shown in the following, due to selection rules, not all states are accessible by the transition. When the electromagnetic field is linearly polarized, only the final states with $M = -1$, $M = 0$, and $M = +1$ can be populated; with a circularly polarized field, the states involved by the transition are those with $M = -2$, $M = -1$, $M = 0$ or $M = 0$, $M = +1$, $M = +2$,

depending on whether the field is right or left circularly polarized. In any case, only three of the five final states can be reached by the transition; thus only nine states need to be included.

B. The coordinate system and the geometry of collisions

Due to the lack of spherical symmetry, the population transferred to the final substates during a single collision would depend on the spatial orientation of the trajectory with respect to the quantization axis. We assume a coordinate system whose Z axis is along the electric field component in the linear polarization case, or along the propagation vector for the circular polarization case. The collision plane is determined by the impact parameter vector $\boldsymbol{\rho}$ and the relative velocity vector $\mathbf{v}$. The direction of a particular trajectory is identified by the angle θ formed by the relative velocity $\mathbf{v}$ and the Z axis and by the angle ϕ between the collision plane and the YZ plane. The Y axis is chosen to lie in the plane of the Z axis and $\mathbf{v}$ (see Fig. 2).

The system wave functions as well as the matrix elements for the collisional coupling are evaluated in this XYZ reference frame.

The relative position of the two atoms at time t is identified by the vector $\mathbf{R} \equiv (X, Y, Z)$, where X, Y, and Z are functions of time. The relative motion of the two atoms is assumed to follow a straight-line trajectory, described by classical mechanics. When $\theta = \phi = 0$, the trajectory lies in the YZ plane and is parallel to the Z axis, and we have

$$X(t) = X_0 + v_x(t - t_0) = 0 \tag{4}$$

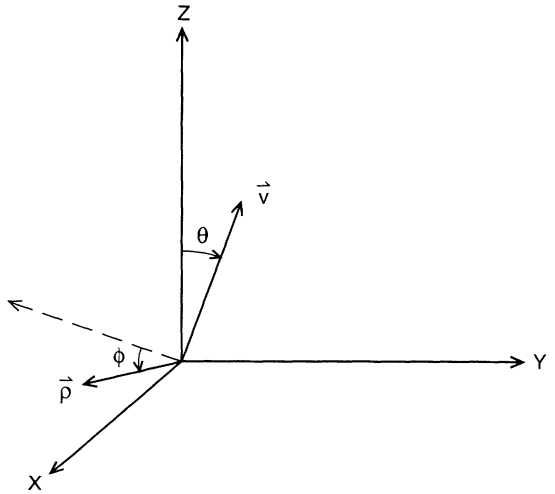

FIG. 2. Laboratory-fixed coordinate system. Z is along electric field vector for linearly polarized radiation and along the propagation direction for circularly polarized radiation. The Y axis is in the plane of Z and relative velocity $\mathbf{v}$. The impact parameters $\boldsymbol{\rho}$ and $\mathbf{v}$ determine the collision plane, which makes an angle ϕ with the YZ plane.

$$Y(t) = Y_0 + v_y(t - t_0) = |\boldsymbol{\rho}| \tag{5}$$

$$Z(t) = Z_0 + v_z(t - t_0), \tag{6}$$

where X_0, Y_0, and Z_0 are the coordinates of the vector $\mathbf{R}$ at the time t_0, chosen so large in magnitude that the two atoms are very far apart and their collisional interaction is negligible. For that particular trajectory, $X_0 = 0$ and $Y_0 = |\boldsymbol{\rho}|$, and the vector $\mathbf{v}$ has only the Z component different from zero.

To pass from this trajectory to another trajectory characterized by arbitrary angles θ and ϕ, we subject each of the two vectors (X_0, Y_0, Z_0) and $\mathbf{v}$ to a rotation by an angle θ about the X axis, followed by another rotation by an angle ϕ about the direction of the $\mathbf{v}$ displaced by the first rotation. Along the trajectory so obtained, the $\mathbf{R}$ joining the two atoms at the time t is given by

$$X(t) = X_0' + v_x'(t - t_0), \tag{7}$$

$$Y(t) = Y_0' + v_y'(t - t_0), \tag{8}$$

$$Z(t) = Z_0' + v_z'(t - t_0), \tag{9}$$

where (X_0', Y_0', Z_0') and $\mathbf{v}'$ are the rotated vectors. Since the second rotation clearly leaves the vector $\mathbf{v}$ unchanged, the relative velocity lies in the YZ plane for any θ and ϕ, hence $v_x' = 0$.

C. Equations of motion

The total wave function of the atomic system is a linear superposition of the nine states involved in the process. We have

$$\Psi(t) = \sum_{j=1}^{9} b_j |j\rangle e^{-i\epsilon_j t}, \tag{10}$$

where ϵ_j is the energy of state j, and

$$H_0|j\rangle = \epsilon_j|j\rangle. \tag{11}$$

All quantities are in atomic units, unless otherwise specified. The wave function of the system evolves with time according to the Schrödinger equation

$$i\frac{\partial \Psi}{\partial t} = H\Psi = (H_0 + H_c + H_r)\Psi, \tag{12}$$

where H_0, H_c, and H_r represent the unperturbed Hamiltonian, the collisional interaction potential, and the radiative coupling, respectively. When the expansion of Ψ in the basis states $|j\rangle$ is used, the Schrödinger equation gives the equations of motion for the coefficients b_j in the expansion

$$\dot{b}_j = -i \sum_{j'=1}^{9} \langle j|H_c + H_r|j'\rangle b_{j'}\, e^{-i(\epsilon_{j'}-\epsilon_j)t} \equiv \sum_{j'=1}^{9} A_{jj'} b_{j'}. \quad (13)$$

This is a system of nine, first-order linear differential equations that must be solved by integration from $t = t_0$ to $t = t_1$, where t_0 and t_1 are properly chosen to be the times prior to and after the collisional interaction. Usually, the origin of time is chosen at the point of closest separation of the two atoms, and t_0, t_1 are symmetrically placed with respect to this point, $t_0 = -t_1$.

The dipole-dipole collisional interaction H_c is given by the sum of four terms, each representing the dipole-dipole coupling of one electron in europium to one electron in strontium

$$H_c = H_{dd}(\mathbf{r}_{a_1}, \mathbf{r}_{b_1}) + H_{dd}(\mathbf{r}_{a_1}, \mathbf{r}_{b_2}) + H_{dd}(\mathbf{r}_{a_2}, \mathbf{r}_{b_1}) + H_{dd}(\mathbf{r}_{a_2}, \mathbf{r}_{b_2}) \quad (14)$$

with

$$H_{dd}(\mathbf{r}_a, \mathbf{r}_b) = \frac{1}{R^3}\left\{\mathbf{r}_a \cdot \mathbf{r}_b - 3(\mathbf{r}_a \cdot \hat{\mathbf{R}})(\mathbf{r}_b \cdot \hat{\mathbf{R}})\right\}, \quad (15)$$

where R represents the distance of the two atoms and $\hat{\mathbf{R}}$ is the unit vector in the direction joining the two atoms.

The operator $H_{dd}(\mathbf{r}_a, \mathbf{r}_b)$ is conveniently expressed in terms of the irreducible tensor operators $Y_1(\theta_a\phi_a)$, $Y_1(\theta_b\phi_b)$ and $Y_1(\Theta\Phi)$ of the angular electrons coordinates θ_a, ϕ_a and θ_b, ϕ_b and the interatomic separation Θ, Φ as

$$H_{dd}(\mathbf{r}_a, \mathbf{r}_b) = \frac{4\pi}{3R^3} r_a r_b \left\{ \sum_{q=-1}^{1} Y^*_{1q}(\theta_a\phi_a) Y_{1q}(\theta_b\phi_b) - 4\pi \left(\sum_{q=-1}^{1} Y^*_{1q}(\theta_a\phi_a) Y_{1q}(\Theta\Phi) \right) \times \left(\sum_{q=-1}^{1} Y^*_{1q}(\theta_b\phi_b) Y_{1q}(\Theta\Phi) \right) \right\}. \quad (16)$$

The expression of the matrix elements of $H_{dd}(\mathbf{r}_a, \mathbf{r}_b)$ between two single-electron states $|u_{6s}(\mathbf{r}_a) v_{5p}(\mathbf{r}_b)\rangle$ and $|u_{6p}(\mathbf{r}_a) v_{5s}(\mathbf{r}_b)\rangle$ are presented in Appendix A. From these elements, one can find the collisional coupling terms among the states by using the expression for the compound states in the LICET process, Eqs. (1) and (2).

The radiative coupling H_r is

$$H_r = \mathbf{E} \cdot (\mathbf{r}_{a_1} + \mathbf{r}_{a_2} + \mathbf{r}_{b_1} + \mathbf{r}_{b_2}), \quad (17)$$

but can be simplified to

$$H_r = \mathbf{E} \cdot (\mathbf{r}_{b_1} + \mathbf{r}_{b_2}) \quad (18)$$

since only the strontium atom has a transition close to resonance with the laser field. In this equation, $\mathbf{E}$ represents the electric component of the electromagnetic field, which couples to the dipole moment of the Sr atom. We must consider the linear polarization and the circular polarization cases separately. In the linear polarization case, $\mathbf{E}$ is directed along the Z axis, and the radiative coupling is written as

$$H_r = E_0 (z_{b_1} + z_{b_2}) \cos \Omega t. \quad (19)$$

In the circular polarization case, the electromagnetic field propagates along the Z axis, and the electric field vector rotates in the XY plane. The radiative coupling is written as

$$H_r = E_0 \frac{(x_{b_1} + x_{b_2}) \cos \Omega t + (y_{b_1} + y_{b_2}) \sin \Omega t}{\sqrt{2}} \quad (20)$$

or, also,

$$H_r = E_0 \frac{(\gamma_{b_1} + \gamma_{b_2}) e^{i\Omega t} + (\gamma^*_{b_1} + \gamma^*_{b_2}) e^{-i\Omega t}}{2\sqrt{2}}, \quad (21)$$

where

$$\gamma_{b_k} = x_{b_k} - i y_{b_k} \quad (k = 1, 2) \quad (22)$$

and the asterisk denotes the complex conjugate.

In both cases of polarization, the rotating wave approximation can be used to eliminate the counter-rotating component of the electric field.

The electromagnetic field couples different sublevels in the two cases. When the field is linearly polarized, the final sublevels 8, 9, and 10 are coupled to the levels 4, 5, and 6, respectively, according to the selection rule $\Delta M = 0$. In the circular polarization case, the final sublevels coupled by the field are 9, 10, and 11, $\Delta M = +1$. The matrix elements of H_r for the two cases are shown in Appendix B.

III. RESULTS

A. Evaluation of the LICET spectra

The LICET process is initiated with europium atoms in the excited state $6s6p\ P_{9/2}$ and strontium atoms in the ground state $5s^2\ ^1S_0$. The compound atomic states corresponding to this initial preparation are states 1, 2, and 3, with $M = -1$, $M = 0$, and $M = +1$, respectively. For fixed field parameters and a given collisional trajectory, we integrate the system (13) of nine differential equations for the state amplitudes b_j, starting from each initial sublevel, i.e., we perform three integrations, one with the initial condition $b_1(-\infty) = 1$ and all other state amplitudes set to zero, one with $b_2(-\infty) = 1$, and one with $b_3(-\infty) = 1$. The transition probability is then found by summing over the final level populations and averaging over the initial conditions so chosen.

It should be noted that we are calculating transition probabilities of a quantum mechanical process, in which interference effects may play a major role. In other words, the population of the final levels, after a process started from a state in which all three initial states are equally populated, may differ from the population aver-

aged over the three initial conditions mentioned above. This is even more evident in the strong-field regime.

The preparation of the initial state of the LICET process in most experiments results in an incoherent superposition of the initial sublevels, in which the three states have random phases. The final level probabilities should then be averaged over the phases of the three initial levels rather than over their populations. However, this procedure would require a much longer computational time. We do not believe that our method of averaging would introduce any substantial error in the determination of the LICET cross section.

Since the process lacks spherical symmetry, the final level probabilities thus evaluated would depend on the geometry of the trajectory. As mentioned in Sec. II B, we have chosen a coordinate system in which the Z axis lies along the polarization axis or the field propagation axis, depending on the polarization of the field. The trajectory of the relative motion can have any orientation in that coordinate system, and one has to average the final level probabilities over the angles θ and ϕ that characterize such orientation (see Sec. II B). We will describe below a method that allows a substantial reduction of the number of cases that need be evaluated.

At the end of these processes, we obtain the final level probability $P(\rho)$, averaged over the initial states, for a given impact parameter ρ and fixed field parameters. The cross section is then obtained by integrating $P(\rho)$ over the impact parameter ρ

$$\sigma = 2\pi \int_0^\infty P(\rho)\rho d\rho . \tag{23}$$

In practice the lower limit $\rho = 0$ is replaced by a finite value, say $\rho = 10$. This has no appreciable effect on the total integral since the major contributions come from much larger impact parameters. We have also put in the physical constraint that the straight-line path is replaced by one representing specular reflection at a hard sphere radius, say $R_0 = 10$, and this gives essentially the same results as taking $\rho = R_0$ as the lower limit.

B. Symmetry considerations

Averaging the probabilities of the final levels over the trajectory parameters θ and ϕ would, in principle, require integrating the system of differential equations for several values of θ ranging from 0° to 180° and ϕ ranging from 0° to 360°. However, as will be shown now, not all of these calculations are necessary. The final level probability turns out to be the same for different sets of θ and ϕ if these angles are related by some symmetry operation. We describe these symmetries in terms of "transfer matrices," defined below. There are three sets of states: the "initial states" (1, 2, and 3), the "intermediate" states (4, 5, and 6), and the "final" states (8, 9, and 10 for the linear polarization case, or 9, 10, and 11 for the circular polarization case, see Appendix B). For each set, we build a three-dimensional vector whose elements are the populations of the states in that set. The first element in each vector is the population of the state with the lowest magnetic quantum number M (usually -1), and the other elements are arranged in the order of increasing values of m. Label I will denote a vector of populations in initial states; labels X and F will denote vectors for the intermediate and final states, respectively.

Because of our choice of the initial conditions, at the initial time $t = t_0$ (with t_0 very large and negative to be considered "$-\infty$") the vector of the initial state population $\mathbf{w}_I$ can only take one of the values

$$\mathbf{w}_I(t_0) = \begin{pmatrix} 1 \\ 0 \\ 0 \end{pmatrix}, \begin{pmatrix} 0 \\ 1 \\ 0 \end{pmatrix}, \begin{pmatrix} 0 \\ 0 \\ 1 \end{pmatrix}, \tag{24}$$

depending on whether the populated state at the initial time is the one with $M = -1$, $M = 0$, or $M = +1$, respectively. At the initial time the two other vectors, $\mathbf{w}_X(t_0)$ and $\mathbf{w}_F(t_0)$ are both $(0,0,0)$.

At the final time, $t = t_1$ (with t_1 large and positive to be considered "$+\infty$"), all vectors contain elements which, in general, are different from zero, and can be related to $\mathbf{w}_I(t_0)$ by means of the transformations

$$\mathbf{w}_j(t_1) = \mathbf{T}_j(t_0, t_1, \theta, \phi)\mathbf{w}_I(t_0) \quad (j = I, X, F), \tag{25}$$

where $\mathbf{T}_j(t_0, t_1, \theta, \phi)$ is a 3×3 matrix, i.e., the transfer matrix for that set of levels.

The transfer matrix is a convenient tool to describe how populations have been transferred by the LICET process from states 1, 2, or 3 at $t = t_0$ to each state of the system at $t = t_1$. To evaluate the transfer matrices, we integrate the system of differential equations (13) with the initial condition $b_j(t_0) = \delta_{j,1}$. The probabilities of the nine states at the end of the integration form the first columns of the matrices $\mathbf{T}_I$, $\mathbf{T}_X$, and $\mathbf{T}_F$, respectively. Then we repeat the integration with $b_j(t_0) = \delta_{j,2}$ to find the second columns of these matrices, and finally we integrate the system with $b_j(t_0) = \delta_{j,3}$ to find the third columns. The dependence of the transfer matrices on the angles θ and ϕ has been made explicit by including these angles in the argument list. The two other arguments, the initial and final times, will be dropped henceforth.

The three transfer matrices, $\mathbf{T}_I(\theta, \phi)$ for the initial states, $\mathbf{T}_X(\theta, \phi)$ for the intermediate states, and $\mathbf{T}_F(\theta, \phi)$ for the final states, are borrowed from the theory of linear transformations. However, as discussed above, our problem is not linear, so that the populations at the final time are not obtainable from Eq. (25) when LICET is started from an arbitrary superposition of $M = -1$, $M = 0$, and $M = +1$ initial states. Thus, these matrices are used here only as a suitable means for describing the symmetries of the problem.

We have considered eight transformations of the original orientation angles of a given collision with θ_0, ϕ_0 characterizing $\mathbf{v}$ and $\boldsymbol{\rho}$:

(a) $\theta = \theta_0, \phi = \phi_0$,
(b) $\theta = \theta_0, \phi = -\phi_0$,
(c) $\theta = 180° - \theta_0, \phi = \phi_0$,

(d) $\theta = \theta_0, \phi = 180^\circ - \phi_0$,
(e) $\theta = \theta_0, \phi = 180^\circ + \phi_0$,
(f) $\theta = 180^\circ - \theta_0, \phi = 180^\circ - \phi_0$,
(g) $\theta = 180^\circ - \theta_0, \phi = -\phi_0$,
(h) $\theta = 180^\circ - \theta_0, \phi = 180^\circ + \phi_0$.

Each combination can be thought of as the result of one or several "elementary" symmetry operations performed on the first set. These symmetry operations are $\phi_0 \to -\phi_0$, $\theta_0 \to 180^\circ - \theta_0$, and $\phi_0 \to 180^\circ + \phi_0$. We now discuss the symmetry properties of our problem in detail.

C. Symmetries in the absence of the laser field

We have found that the transfer matrices for the initial states, in cases (b) through (h), are related to the transfer matrix of case (a) by simple algebraic transformations. Namely,

$$\mathbf{T}_I(\theta_0, \phi_0) = \mathbf{T}_I(\theta_0, \phi_0), \tag{26a}$$

$$\mathbf{T}_I(\theta_0, -\phi_0) = \mathbf{Y}^{-1}\mathbf{T}_I(\theta_0, \phi_0)\mathbf{Y}, \tag{26b}$$

$$\mathbf{T}_I(180^\circ - \theta_0, \phi_0) = \{\mathbf{T}_I(\theta_0, \phi_0)\}^t, \tag{26c}$$

$$\mathbf{T}_I(\theta_0, 180^\circ - \phi_0) = \{\mathbf{T}_I(\theta_0, \phi_0)\}^t, \tag{26d}$$

$$\mathbf{T}_I(\theta_0, 180^\circ + \phi_0) = \{\mathbf{Y}^{-1}\mathbf{T}_I(\theta_0, \phi_0)\mathbf{T}\}^t, \tag{26e}$$

$$\mathbf{T}_I(180^\circ - \theta_0, 180^\circ - \phi_0) = \mathbf{T}_I(\theta_0, \phi_0), \tag{26f}$$

$$\mathbf{T}_I(180^\circ - \theta_0, -\phi_0) = \{\mathbf{Y}^{-1}\mathbf{T}_I(\theta_0, \phi_0)\mathbf{T}\}^t, \tag{26g}$$

$$\mathbf{T}_I(180^\circ - \theta_0, 180^\circ + \phi_0) = \mathbf{Y}^{-1}\mathbf{T}_I(\theta_0, \phi_0)\mathbf{T}, \tag{26h}$$

where $\{\ \}^t$ denotes the transpose matrix, and

$$\mathbf{Y} = \begin{pmatrix} 0 & 0 & 1 \\ 0 & 1 & 0 \\ 1 & 0 & 0 \end{pmatrix}. \tag{27}$$

Note that $\mathbf{Y}$ is equal to its inverse $\mathbf{Y}$. In relations (26) we have included also the trivial relation (26a) for completeness.

If one transformation $(\theta_0, \phi_0) \to (\theta_1, \phi_1)$ is the result of two elementary transformations, the transfer matrix transforms according to the product of these two transformations. For instance, the transformation $(\theta_0, \phi_0) \to (180^\circ - \theta_0, -\phi_0)$ is the result of $(\theta_0, \phi_0) \to (180^\circ - \theta_0, \phi_0)$ and $(\theta_0, \phi_0) \to (\theta_0, -\phi_0)$; accordingly, the transfer matrix for $(180^\circ - \theta_0, -\phi_0)$ is obtained from the transfer matrix for (θ_0, ϕ_0) by taking the transpose (transformation $\theta_0, \phi_0 \to 180^\circ - \theta_0, \phi_0$) of $\mathbf{Y}^{-1}\mathbf{T}_I(\theta_0, \phi_0)\mathbf{Y}$ (transformation $\theta_0, \phi_0 \to \theta_0, -\phi_0$).

Because of the properties described above, these transformations $(\theta_0, \phi_0) \to (\theta_1, \phi_1)$ form a group, and the transfer matrices are a representation of this group. Transformation (26a) can be assumed to represent the identity element in the group.

The elements of this group can be divided into subgroups, and this can be done in several ways.

(i) The subgroups of elements related by the operation of transposition: there are two such subgroups, one formed by transformations (a), (c), (d), and (f) and the other formed by the transformations (b), (e), (g), and (h). We pass from an element in one subgroup to an element in the other subgroup by performing a $\mathbf{Y}$ transformation.

(ii) The subgroups formed by elements related by the $\mathbf{Y}$ transformation: there are two such subgroups, one formed by the transformations (a), (b), (f), and (h) and the other formed by the elements (c), (d), (e), and (g). We pass from an element in one subgroup to an element in the other subgroup by performing a transposition.

Since the transpose of the transpose of a matrix coincides with the matrix itself, and the matrix $\mathbf{Y}$ is the inverse of itself (i.e., $\mathbf{Y}^2$ is the identity matrix), there are elements within each subgroup (i) and (ii) that are equal. Thus, there is a third way of dividing elements into subgroups, namely the subgroups of elements related by the identity matrix, i.e.,

(iii) the subgroups of equal elements. There are four such subgroups, formed by transformations (a) and (f); (b) and (h); (c) and (d); (e) and (g).

This is the classification scheme for the symmetry properties of the initial state transfer matrix in the absence of the field.

D. Symmetry properties with linearly or circularly polarized fields

1. Linear polarization case

In the LICET process with linearly polarized field, the symmetry properties of the transfer matrix for the initial states are the same as those described above for the "no field" case, while the transfer matrix for the final states keeps only those symmetry properties within groups (ii) and (iii) above. In other words, $\mathbf{T}_F(\theta_0, \phi_0)$ does not possess the symmetry properties associated with transpositions, but does possess symmetry properties associated with $\mathbf{Y}$ transformations: each transformation in the group (a), (b), (f), (h) can be obtained from another one of the same group by performing on it one or more $\mathbf{Y}$ transformations; the same is true for a transformation in the group (c), (d), (e), (g). But there is no transformation which, when acted upon by an element of the first group, transforms it into an element of the second group (or vice versa).

Within each subgroup there are elements that are equal (elements (a), (f) and elements (b), (h) in the first group; elements (c), (d) and elements (e), (g) in the second one, see discussion above).

2. *Circular polarization case*

In the LICET process with a circularly polarized field, the initial state transfer matrix $\mathbf{T}_I(\theta,\phi)$ keeps only those symmetry properties within groups (i) and (iii) above. Thus, in this case, $\mathbf{T}_I(\theta_0,\phi_0)$ does not possess the symmetry properties that are associated to $\mathbf{Y}$ transformations, but does possess symmetry properties associated with transposition.

Also the final level transfer matrix loses some symmetry properties with respect to the linearly polarized case: in the circular polarization case, $\mathbf{T}_F(\theta,\phi)$ keeps only those symmetries associated to the identity transformations of groups (iii) above. Thus, cases (a) and (f) yield the same transfer matrix, and so do cases (b), (h), cases (c), (d) and cases (e), (g) (see discussion above).

For instance, $\mathbf{T}_F(180^\circ-\theta_0,180^\circ-\phi_0)=\mathbf{T}_F(\theta_0,\phi_0)$, and also $\mathbf{T}_F(180^\circ-\theta_0,180^\circ+\phi_0)=\mathbf{T}_F(\theta_0,-\phi_0)$, but there is no way of relating the outcome at $180^\circ-\theta_0,\phi_0$ to the outcome at θ_0, ϕ_0.

This discussion of the symmetry properties of the transfer matrices allows us to reduce the ranges of θ and ϕ for which the integration of the system (13) is required. Indeed, the average of the final level probabilities over the initial preparation of states $M=-1$, $M=0$, $M=+1$, is just one third of the sum of all nine elements in the transfer matrix $\mathbf{T}_F(\theta,\phi)$. The symmetry operations of transposition and $\mathbf{Y}$ transformations keep the sum unchanged. Therefore, if we find that $\mathbf{T}_F(\theta_1,\phi_1)$ is related to $\mathbf{T}_F(\theta_0,\phi_0)$ by one of these transformations, we do not need to evaluate the transition probability at θ_1,ϕ_1, if we know the transition probability at θ_0,ϕ_0. Hence, we can restrict the ranges of the trajectory angles to the following:

For linear polarization, we can restrict integration to the ranges $0^\circ\le\theta\le 90^\circ$ and $0^\circ\le\phi\le 180^\circ$. For circular polarization, we can restrict integration to the ranges $0^\circ\le\theta\le 90^\circ$ and $-180^\circ\le\phi\le 180^\circ$. These ranges can be deduced by the symmetry properties of the final level transfer matrix $\mathbf{T}_F(\theta,\phi)$. However, we can also exploit the symmetry properties of the initial level transfer matrix $\mathbf{T}_I(\theta,\phi)$ to further reduce the ranges of integration. We know that the intermediate states 4, 5, and 6 are just populated adiabatically during the collisional process. At the end of a LICET transition, population has been transferred only to the final levels, and little remains in the intermediate states. Thus, we expect the matrix elements of $\mathbf{T}_X(\theta,\phi)$ to be small compared to the matrix elements in $\mathbf{T}_I(\theta,\phi)$ and $\mathbf{T}_F(\theta,\phi)$. On the other hand, the sum of all elements in the three transfer matrices is equal to three, due to conservation of populations. These two facts allow us to state that the sum of elements in $\mathbf{T}_F(\theta,\phi)$ remains almost constant when passing from θ_0, ϕ_0 to θ_1, ϕ_1, even if the corresponding $\mathbf{T}_I(\theta,\phi)$, but not $\mathbf{T}_F(\theta,\phi)$, are related by a symmetry operation. To elucidate this point with an example, let us consider, the case of linear polarization. The transfer matrix $\mathbf{T}_I(\theta,\phi)$ resulting from an integration at $\theta=\theta_0$, $\phi=180^\circ-\phi_0$ is the transpose of the matrix $\mathbf{T}_I(\theta,\phi)$ resulting from an integration at $\theta=\theta_0$, $\phi=\phi_0$, while the corresponding matrices $\mathbf{T}_F(\theta,\phi)$ do not exhibit any symmetry properties. Thus, the sum of the elements of $\mathbf{T}_I(\theta,\phi)$ remains constant; and, because of conservation of total population, so does the sum of elements in $\mathbf{T}_F(\theta,\phi)$ if we can neglect the population transferred to the intermediate states. We refer to this property as a "quasisymmetry" property. Note that these "quasisymmetries" appear only in the average of the final level population over the initial states.

Usually, the final population in the intermediate levels has been found to be two to three orders of magnitude smaller than that in the final levels. Thus, with a minor loss in accuracy, we can further reduce the ranges of integration in the two cases: For linear polarization, integration can be reduced to the ranges $0^\circ\le\theta\le 90^\circ$ and $0^\circ\le\phi\le 90^\circ$. For circular polarization, integration can be reduced to the ranges $0^\circ\le\theta\le 90^\circ$ and $-90^\circ\le\phi\le 90^\circ$.

E. The calculated spectra

We have calculated the spectral profiles in the high-intensity regime, for both linear and circular polarization of the laser field. The field intensity in both cases was chosen to be 10^8 W/cm^2 and the relative speed of the collision was taken to be 5×10^4 cm/s. The radial dipole matrix elements are taken to be the values given by the Bates-Damgaard approximation: $(5s|r|5p)_{\mathrm{Sr}}=3.82$ a.u. and $(6s|r|6p)_{\mathrm{Eu}}=3.77$ a.u.

Figure 3 is a graph of the spectral profile for linear polarization. In this case, the peak is shifted, with respect to the bare atomic resonance, by the ac Stark effect. The shift is of the same magnitude as in the spectral profile obtained under the approximation where magnetic degeneracy is neglected [12,13]. The line shape shown in Fig. 3 was obtained by averaging over the spatial distribution of trajectories and the three initial substates, as discussed above.

It should be noted, however, that the spectral profile obtained when LICET is started from a single magnetic substate shows a more structured shape. In Fig. 4 we

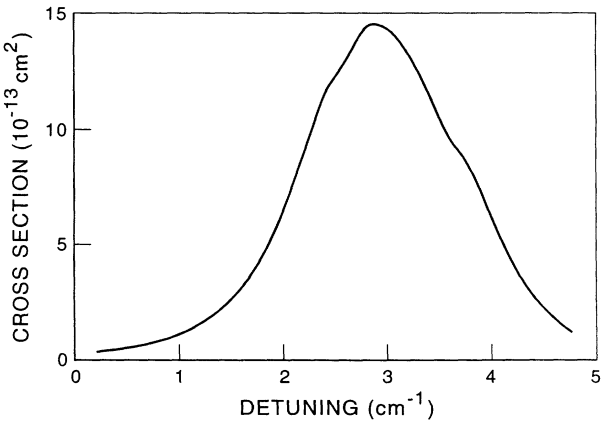

FIG. 3. LICET spectral line shape for linearly polarized radiation, including all M states (nine states) and averaging over initial M, and the θ and ϕ trajectory parameters.

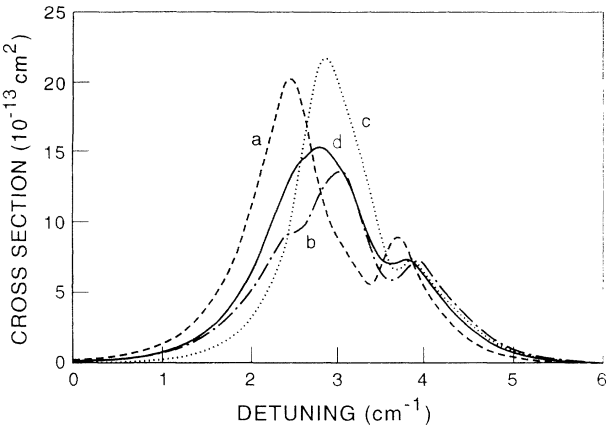

FIG. 4. LICET spectral line shapes for linear polarization including all M states, both trajectory parameters $\theta = 60°$ and $\phi = 30°$, and initial M state; (a) $M = -1$, (b) $M = 0$, (c) $M = 1$, (d) average over M.

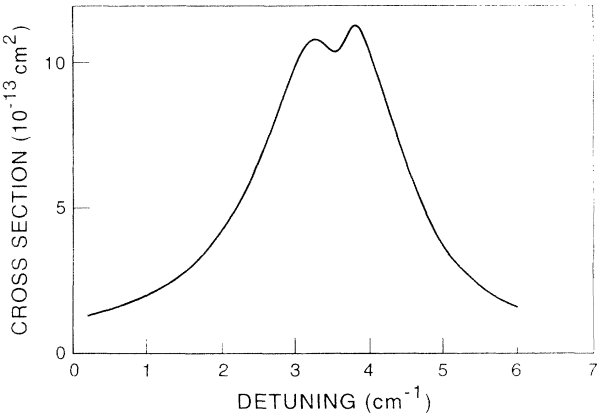

FIG. 5. LICET spectral line shape for linearly polarized radiation and only three basis states ($M = 0$), including averaging over the θ and ϕ trajectory parameters.

show profiles of the LICET spectrum when the process is initiated from each of the substates 1, 2, and 3 ($M = -1$, 0, and $+1$, respectively). Moreover, no average is done over the space orientation of the trajectory, i.e., the angles that characterize the collision geometry are kept fixed at $\theta = 30°$ and $\phi = 60°$.

The two-peak structure that appears in Fig. 4, curves (a), (b), (c), can be explained in the following way: the ac Stark shift depends on the atom-field coupling, and according to Eqs. (B1)–(B3), is different for the strontium transitions $5s5p\,^1P_1(M = \pm 1) \leftrightarrow 5p^2\,^1D_2(M = \pm 1)$ and $5s5p\,^1P_1(M = 0) \leftrightarrow 5p^2\,^1D_2(M = 0)$. This determines the appearance of two peaks in the spectral profile.

Curve (d) in Fig. 4 shows the arithmetic mean of these profiles, i.e., their average over the initial substates. Although obtained for a single orientation of the trajectory, this graph is remarkably similar to the line shape in Fig. 3. The two-peak structure in curves (a), (b), and (c) is smoothed down in the process of averaging over the initial states.

To see the effect of the collision geometry alone, we have also recalculated the spectral profile for the linear polarization case under the assumption that the magnetic degeneracy of the sublevels is limited to the $M = 0$ substates alone in each of the initial, intermediate, and final states of the LICET process. Under this assumption, therefore, the population is distributed among three states only. The corresponding graph is shown in Fig. 5. Strangely enough, the line shape in this approximation also shows a two-peak profile. Both peaks of the spectral profile are lower than in the previous case (Fig. 3), but the shift is larger. It must be noted that the spectral profile in Ref. [12] was found by integrating over collisions occurring in the plane orthogonal to the direction of the field polarization (i.e., collision trajectories characterized by $\theta = 90°$), while the graph of Fig. 5 was obtained by averaging the $(M = 0) \leftrightarrow (M = 0)$ transition probabilities over collisions occurring with any orientation in space. This seems to indicate that a structure in the spectral profile can be introduced by the collisional geometry alone.

In Fig. 6 we illustrate the spectral line profile for the LICET process with circular polarization of the laser field. In this case the spectral profile departs substantially from the profile obtained with linearly polarized fields. The spectrum is much wider and again presents a two-peaked structure, but its width is twice as large and its center of mass is detuned from resonance by 30% more than in the linear polarization case.

The wider spectral profile is attributable to the factor 6 difference in the ac Stark shift for the transitions $(M = -1) \leftrightarrow (M = 0)$ and $(M = +1) \leftrightarrow (M = +2)$, see Eqs. (B4) and (B6). All radiative coupling coefficients are different in the circular polarization case, while in the linear polarization case two of them are equal. This, according to the discussion above, should give rise to a three-peak spectrum with circular polarization corresponding to the three different shifts induced by the ac Stark effect. That this is actually the case is shown in Fig. 7, where curves

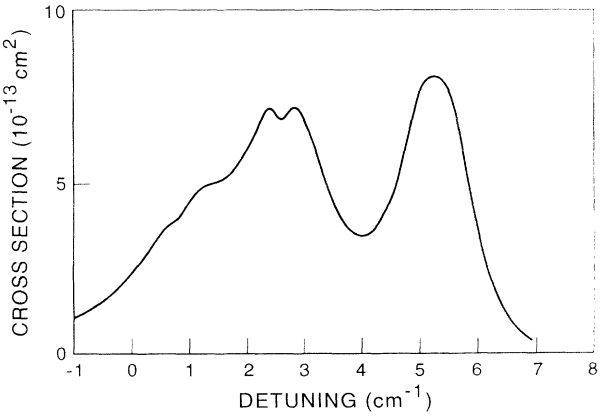

FIG. 6. LICET spectral line shape for circularly polarized radiation, including all M states and averaging over initial M, and the θ and ϕ trajectory parameters.

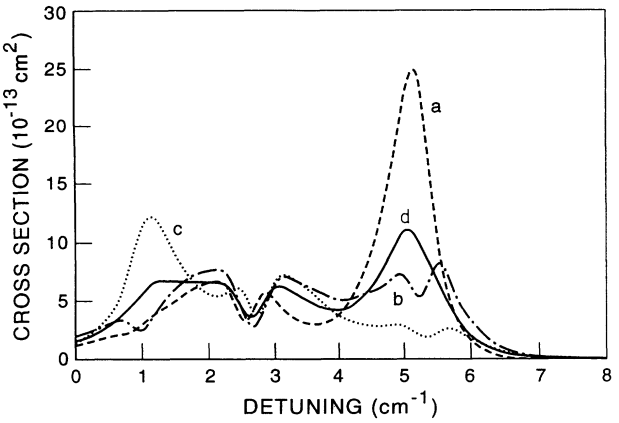

FIG. 7. LICET spectral line shapes for circularly polarized radiation, including all M states for the trajectory parameters $\theta = 60°$ and $\theta = 30°$, and initial M state; (a) $M = -1$, (b) $M = 0$, (c) $M = 1$, (d) average over M.

(a), (b), and (c) illustrate spectral profiles for each of the initial sublevels $M = -1$, 0, and $+1$ and for a fixed orientation of the trajectory ($\theta = 30°$, $\theta = 60°$). The arithmetic mean of those profiles is shown in panel (d).

From Fig. 7, we see that the spectral profile that results from an initial preparation in a single magnetic substate consists of three peaks. Moreover, holes are burned into the shape by interference effects between adjacent transitions, so that the overall spectral profile shows a much richer structure. These interference effects are present also in the spectral profiles for the linear polarization case [Figs. 4(a)–(c)], but are less evident.

Finally, in Fig. 8 we present three curves that show how population is distributed among the final sublevels at the end of the LICET process with circular polarization, at different laser frequencies. The transition probability is plotted vs the impact parameter ρ for three different values of the detuning, which were chosen to match the ac Stark shift for the three different transitions. In these figures, the orientation of the trajectory is again fixed at $\theta = 30°$, $\theta = 60°$.

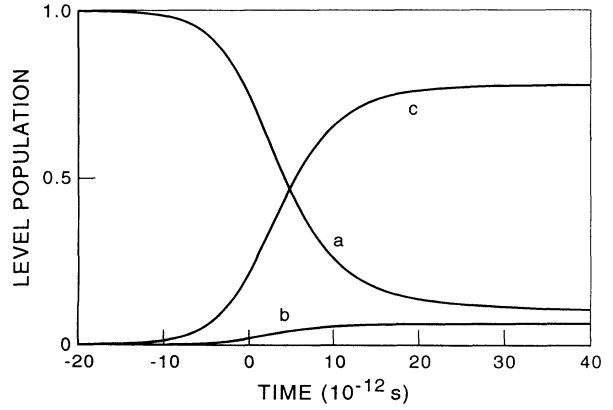

FIG. 8. Typical time evolution of level populations (summed over M states) for the (a) initial, (b) intermediate, and (c) final states during this LICET process.

In Fig. 8(a), the laser frequency is detuned from the "bare" atomic resonance by 0.69 cm^{-1}, which corresponds to the expected Stark shift of the strontium transition $5s5p\ ^1P_1(M = -1) \leftrightarrow 5p^2\ ^1D_2(M = -2)$ for a laser intensity of 10^8 W/cm^2. In this case, only the final substate with $M = -2$ gets the highest population at large values of the impact parameter, which contribute mostly to the spectral line shape. Similarly, in (b) and (c), the laser frequency was detuned from resonance by 2.18 cm^{-1} and 5.44 cm^{-1}, respectively, corresponding to the expected Stark shifts for the transitions $5s5p\ ^1P_1(M = 0) \leftrightarrow 5p^2\ ^1D_2(M = -1)$ and $5s5p\ ^1P_1(M = 1) \leftrightarrow 5p^2\ ^1D_2(M = 0)$. In Fig. 8(b), the final substate that is mostly populated in collisions with large impact parameters is state 8, while in Fig. 8(c) it is state 9. These graphs confirm the explanation given above of the multiple peak structure of the LICET spectra obtained with polarized fields.

IV. CONCLUSIONS

We have calculated the spectral profiles of LICET processes induced by polarized, high-intensity laser fields. The graphs presented in this article refer to the vapor mixtures of europium and strontium, and show the line shapes near resonance. The laser intensity is the same in all graphs, namely 10^8 W/cm^2.

The spectra in Figs. 3 and 6 were obtained for linear and circular polarizations, respectively, by averaging over the initial states and summing over the final states. Calculations were performed on a nine-state approximation of the electronic excited states of the quasimolecule formed during the collision and assuming straight-line trajectories. Due to the lack of spherical symmetry in the interactions between the two atoms and in the interaction of the system with the electromagnetic field, a full three-dimensional geometry for the collision was introduced and the spectra were averaged over all possible orientations of the trajectory of relative motion.

These spectra show a structured line shape, which was not present in the high-intensity profiles obtained in previous calculations, in which magnetic degeneracy was neglected. However, also in the present cases, the spectra have their peak occurring at laser frequencies displaced from the unperturbed atomic resonance, toward the antistatic side of the curve. We have shown that both the shift of the peak and the structure in the spectra can be explained in terms of the ac Stark effect, which acts in a different way on transitions with different coupling coefficients. Averaging over the initial states and trajectory orientations removes much of the structure in the spectra but does not eliminate the large spectral width. The resulting spectra, therefore, show spectral widths that differ substantially from the widths inferred from previous models that used only an $M = 0$ basis set and linearly polarized light. The spectrum obtained with circular polarization is wider than that obtained with linear polarization, but the overall shape in both cases is in

agreement with what one would expect from a superposition of two or three shapes, one for each transition having a different value of the coupling coefficients. Some interference effects were also displayed in the spectra obtained from a single substate and a single trajectory orientation, but these effects were washed out in the averaging processes.

Some of these features could be detectable in experiments, especially when using circular polarization, and may help in determining the median position of the spectral shape with respect to the unperturbed LICET atomic resonance.

Also, the present more refined model of the LICET processes, which includes magnetic substates of the atomic system, yields spectral line shapes whose peaks are shifted by the ac Stark effect. In spite of the lack of experimental confirmation, all calculations made up to now agree in predicting a shift of the peak. Its reduction or even elimination, therefore, should be ascribed to effects that were not contained in the existing models, such as the competing decay of the excited strontium atoms due to nonradiative transitions, or the fact that high fields may bring other levels, so far considered as virtual, into the interaction process.

One feature that remains to be explained is the presence of two peaks in the spectrum obtained using a three-state approximation, but allowing for a full three-dimensional description of the collision geometry (see Fig. 5). According to the discussion above, in such an approximation there is just one radiative coupling; hence, a single shifted peak should result. A possible explanation of this could lie in the fact that the shift depends on the collisional parameters that are largest for collisions occurring at very large impact parameters.

We feel that additional refinements to the theory, such as more realistic classical trajectories than straight lines or the inclusion of more atomic states into our basis set, would result in only minor changes in our present LICET cross sections. The main contributions to the overall transition probabilities occur at a large impact parameter ($\sim 50a_0$ to $150a_0$) where the straight-line path should be quite valid, and additional states are too far removed energetically to be expected to be populated — even adiabatically. We have folded a Gaussian spatial distribution of intensities, as would be expected in the experimental [14] transfer laser, into our evaluated $M = 0$ cross sections, but that does not appreciably help the agreement at the high intensities. We are planning to continue the search for an understanding of this discrepancy between theory and experiment.

ACKNOWLEDGMENTS

A.B. would like to thank Professor Edward Robinson for extremely helpful discussions on the ac Stark shift. S.G. has received partial support from the National Science Foundation through Grant No. PHY90-12244 and is grateful for the hospitality of the Istituto di Elettronica Quantistica.

APPENDIX A

In the present model the states coupled by the collisional interaction are 1,2,3 and 4,5,6 (see Sec. II A). The matrix elements of each term in the collisional operator can be written, in conformity with the Wigner-Eckart theorem, as a product of radial matrix elements and Clebsch-Gordan coefficients. For instance, the matrix element of $r_a r_b Y^*_{1q}(\theta_a\phi_a)Y_{1q}(\theta_b\phi_b)$ taken between two compound states $|u_{n_a\ell_a m_a}(\mathbf{r}_a)v_{n_b\ell_b m_b}(\mathbf{r}_b)\rangle$ and $|u_{n'_a\ell'_a m'_a}(\mathbf{r}_a)v_{n'_b\ell'_b m'_b}(\mathbf{r}_b)\rangle$ is given by

$$\left(\frac{3}{4\pi}\right)\left[\frac{(2\ell_a+1)(2\ell_b+1)}{(2\ell'_a+1)(2\ell'_b+1)}\right]^{1/2} C(\ell_a 1\ell'_a;000)C(\ell_b 1\ell'_b;000)$$
$$\times C(\ell_a 1\ell'_a;m_a q m'_a)C(\ell_b 1\ell'_b;m_b q m'_b)$$
$$\times(n_a\ell_a|r_a|n'_a\ell'_a)(n_b\ell_b|r_b|n'_b\ell'_b)\,. \tag{A1}$$

The $(n\ell|r|n'\ell')$ are radial matrix elements for the respective atoms A and B.

The matrix elements of $H_{dd}(\mathbf{r}_a,\mathbf{r}_b)$ are obtained by summing over q the products of Clebsch-Gordan coefficients in the expression (A1), and are given by

$$\langle u_{6s}(\mathbf{r}_a)v_{5p-1}(\mathbf{r}_b)|H_{dd}(\mathbf{r}_a,\mathbf{r}_b)|u_{6p-1}(\mathbf{r}_a)v_{5s}(\mathbf{r}_b)\rangle = \frac{3u_z^2-1}{6R^3}, \tag{A2}$$

$$\langle u_{6s}(\mathbf{r}_a)v_{5p-1}(\mathbf{r}_b)|H_{dd}(\mathbf{r}_a,\mathbf{r}_b)|u_{6p0}(\mathbf{r}_a)v_{5s}(\mathbf{r}_b)\rangle = \frac{-u_z}{\sqrt{2}R^3\,(u_x-iu_y)}, \tag{A3}$$

$$\langle u_{6s}(\mathbf{r}_a)v_{5p-1}(\mathbf{r}_b)|H_{dd}(\mathbf{r}_a,\mathbf{r}_b)|u_{6p+1}(\mathbf{r}_a)v_{5s}(\mathbf{r}_b)\rangle = \frac{(u_x-iu_y)^2}{2R^3}, \tag{A4}$$

$$\langle u_{6s}(\mathbf{r}_a)v_{5p0}(\mathbf{r}_b)|H_{dd}(\mathbf{r}_a,\mathbf{r}_b)|u_{6p-1}(\mathbf{r}_a)v_{5s}(\mathbf{r}_b)\rangle = \frac{-u_z}{\sqrt{2}R^3\,(u_x+iu_y)}, \tag{A5}$$

$$\langle u_{6s}(\mathbf{r}_a)v_{5p0}(\mathbf{r}_b)|H_{dd}(\mathbf{r}_a,\mathbf{r}_b)|u_{6p0}(\mathbf{r}_a)v_{5s}(\mathbf{r}_b)\rangle = \frac{-3u_z^2-1}{3R^3}, \tag{A6}$$

$$\langle u_{6s}(\mathbf{r}_a)v_{5p0}(\mathbf{r}_b)|H_{dd}(\mathbf{r}_a,\mathbf{r}_b)|u_{6p+1}(\mathbf{r}_a)v_{5s}(\mathbf{r}_b)\rangle = \frac{u_z}{\sqrt{2}R^3\,(u_x-iu_y)}, \tag{A7}$$

$$\langle u_{6s}(\mathbf{r}_a)v_{5p+1}(\mathbf{r}_b)|H_{dd}(\mathbf{r}_a,\mathbf{r}_b)|u_{6p-1}(\mathbf{r}_a)v_{5s}(\mathbf{r}_b)\rangle = \frac{(u_x - iu_y)^2}{2R^3}, \tag{A8}$$

$$\langle u_{6s}(\mathbf{r}_a)v_{5p+1}(\mathbf{r}_b)|H_{dd}(\mathbf{r}_a,\mathbf{r}_b)|u_{6p0}(\mathbf{r}_a)v_{5s}(\mathbf{r}_b)\rangle = \frac{u_z}{\sqrt{2}R^3\ (u_x + iu_y)}, \tag{A9}$$

$$\langle u_{6s}(\mathbf{r}_a)v_{5p+1}(\mathbf{r}_b)|H_{dd}(\mathbf{r}_a,\mathbf{r}_b)|u_{6p+1}(\mathbf{r}_a)v_{5s}(\mathbf{r}_b)\rangle = \frac{3u_z^2 - 1}{6R^3}. \tag{A10}$$

In these expressions, we have omitted the radial matrix elements $(5s|r|5p)_{\mathrm{Sr}}$ and $(6s|r|6p)_{\mathrm{Eu}}$ that are common factors to all terms; u_x, u_y, and u_z represent the components of the unit vector $\widehat{\mathbf{R}}$ joining the two atoms, and are expressed in terms of Θ, Φ as

$$u_x = \sin\Theta\cos\Phi, \tag{A11}$$

$$u_y = \sin\Theta\sin\Phi, \tag{A12}$$

$$u_z = \cos\Theta. \tag{A13}$$

The three components u_x, u_y, and u_z of the unit vector joining the two atoms depend on time, and their explicit forms can be found by using Eqs. (7)–(9).

APPENDIX B

These are the matrix elements of the radiative coupling when the field is linearly polarized:

$$\langle 4|H_r|8\rangle = \frac{1}{\sqrt{3}}E_0\cos\Omega t, \tag{B1}$$

$$\langle 5|H_r|9\rangle = \frac{2}{3}E_0\cos\Omega t, \tag{B2}$$

$$\langle 6|H_r|10\rangle = \frac{1}{\sqrt{3}}E_0\cos\Omega t. \tag{B3}$$

In the circular polarization case, the field couples a different set of sublevels:

$$\langle 4|H_r|9\rangle = -\tfrac{1}{6}E_0e^{i\Omega t}, \tag{B4}$$

$$\langle 5|H_r|10\rangle = -\frac{1}{2\sqrt{3}}E_0e^{i\Omega t}, \tag{B5}$$

$$\langle 6|H_r|11\rangle = -\frac{1}{\sqrt{6}}E_0e^{i\Omega t}. \tag{B6}$$

In these expressions, we have omitted the radial matrix element $(5s|r|5p)_{\mathrm{Sr}}$.

It should be noted that in both polarization cases, the final number of sublevels involved in the transition are always three, while the remaining two sublevels are uncoupled by the field interaction and remain empty at all times. Thus, of the original set of eleven states, only nine need be considered in the calculations.

[1] L. I. Gudzenko and S. I. Yakovlenko, Zh. Eksp. Teor. Fiz. **62**, 1686 (1972) [Sov. Phys. JETP 35, 877 (1972)].
[2] S. Geltman, J. Phys. B **9**, L569 (1976).
[3] A. Gallagher and T. Holstein, Phys. Rev. A **16**, 2413 (1977).
[4] A. Bambini and P. Berman, Phys. Rev. A **35**, 3753 (1987).
[5] M. G. Payne, V. E. Anderson, and J. E. Turner, Phys. Rev. A **20**, 1032 (1979).
[6] S. Geltman, Phys. Rev. A **35**, 3775 (1987).
[7] For a review of this work see S. E. Harris, J. F. Young, R. W. Falcon, W. R. Green, D. B. Lidow, J. Lukasik, J. C. White, M. D. Wright, and G. A. Zdasinek, in *Atomic Physics*, edited by D. Kleppner and F. M. Pipkin (Plenum, New York, 1981), Vol. 7, pp. 407–428.
[8] B. Cheron and H. Lemery, Opt. Commun. **42**, 109 (1982).
[9] A. Debarré, J. Phys. B **16**, 432 (1983).
[10] D. Z. Zhang, B. Nikolaus, and P. E. Toschek, Appl. Phys. B **28**, 195 (1981); F. Dorsch, S. Geltman, and P. E. Toschek, Phys. Rev. A **37**, 2441 (1988).
[11] C. Brechignac, Ph. Cahuzac, and P. E. Toschek, Phys. Rev. A **21**, 1969 (1980); A. Debarré, J. Phys. B **15**, 1693 (1982); M. Matera, M. Mazzoni, R. Buffa, S. Cavalieri, and E. Arimondo, Phys. Rev. A **36**, 1471 (1987); M. Matera, M. Mazzoni, M. Bianconi, R. Buffa, and L. Fini, *ibid.* **41**, 3766 (1990).
[12] A. Bambini, M. Matera, A. Agresti, and M. Bianconi, Phys. Rev. A **42**, 6629 (1990).
[13] S. Geltman, Phys. Rev. A **45**, 4792 (1992).
[14] M. Mazzoni and L. Fini, Phys. Rev. A **48**, 3786 (1993).